TÜBİTAK

Turkish Journal of Earth Sciences

http://journals.tubitak.gov.tr/earth/

Research Article

Turkish J Earth Sci
(2021) 30: 1096-1111

doi:10.3906/yer-2106-12

Numerical modeling of fluid flow and heat transfer in Kurşunlu geothermal field-KGF (Salihli, Manisa / Turkey)

Toygar AKAR*, **Ünsal GEMİCİ**, **Melis SOMAY-ALTAŞ**, **Gültekin TARCAN**
Department of Geological Engineering, Dokuz Eylül University, İzmir, Turkey

Received: 14.06.2021 • **Accepted/Published Online:** 16.09.2021 • **Final Version:** 01.12.2021

Abstract: Nowadays, the need for energy is increasing more and more. It is more difficult to acquire new resources in various fields than to preserve existing energy resources. Although Turkey is a very rich state in terms of various energy resources, misuse of these resources can even lead to conflicts that may occur between the states in forthcoming years. In today's economic conditions, we can only protect our energy resources with the correct way of management. In this context, it is very important to reveal the mechanisms that make up the geothermal systems, which are very common in Western Anatolia. In this study, how the fluid circulation mechanism in the geothermal system takes place, and under which conditions the infiltrating water is heated in the Kurşunlu geothermal field (KGF) have been examined. FEFLOW software was used in numerical modeling. Fluid flow and heat transfer equations are solved on a two-dimensional vertical model using FEFLOW software. A variable-width finite element mesh consisting of 55,590 elements was created in this scope. Since triangular meshes are preferred in vertical models, the mesh produced according to the Delaunay method was used. All lateral boundaries are designed as a no-flow boundary condition. For boundary conditions, hydraulic heads on top of the model and temperature values at both the top and bottom of the model are defined. Additionally, initial values were produced for the entire Kurşunlu geothermal system under steady-state conditions, and a transient model was built to run for 700,000 days. The regional flow direction is towards to the North. The fluids are transmitted deeply and heated through fault zones and transported towards the surface. Convective flows start to form below –1000 m altitudes in the fault zones and in the geothermal aquifer widespread convective flows in deeper regions were formed, while smaller spread convective flows were formed near the surface and shallow depths of the aquifer. In the process of convective flow, heated fluids reach to Kurşunlu region and forms the spring. Finally, two more possible high-temperature areas have been identified, indicating that the flow vectors point to the surface.

Key words: Geothermal aquifer, groundwater modeling, fluid flow mechanism, Salihli, FEFLOW

1. Introduction

Geothermal energy is recommended as a renewable resource to meet the world's energy needs, while nonrenewable resources such as fossil fuels are diminishing. The fluid flow in most geothermal systems takes place with faults and fissures. In generally accepted models in fault controlled geothermal systems, the fluid is controlled by both physical and structural properties of the fault. Thus, geothermal systems can also exist in aquifers in low permeability aquifers (Saemundsson et al., 2009). In low permeability units, fracture area is more important than fracture itself (Hofmann et al., 2014; Economides and Nolte, 2000). In this way, the unit shows an aquifer feature even though it has a low permeability. Conversely, when permeability is high enough, deep circulation cells develop on a regional scale (Hochstein et al. 1990). This convective flow controls the fluid flow dynamics and temperature and consequently changes the temperature in the basin and faults (Simms and Garven 2004). Geothermal activity and geological structures control the fluid cycle and, therefore, allow mixing of different types of water. Fluids in these systems have a wide range of chemical composition resulting from the rocks they circulate. Therefore, determination of water-rock relations and possible fluid flow paths of geothermal systems plays an important role in defining fluid dynamics. In the last decade, numerical models of fluid flow and heat transport were increasingly used to improve the understanding of hydrothermal systems and their natural evolution, especially in fractured environments (Magri et al., 2011).

KGF was formed in Gediz Graben in Western Anatolia, Turkey. Gediz Graben is one of the most studied areas by researchers. Tectonic and petrographic studies are particularly common (Erdoğan and Güngör, 1992; Hetzel et al, 1995a; Hetzel et al, 1995b; Seyitoğlu, 1996; Emre, 1996a; Emre, 1996b; Emre and Sözbilir, 1997; Dora et al,

* Correspondence: toygar.akar@deu.edu.tr

1997). Many geological, geophysical, and drilling studies have also been carried out in the region (Yılmazer, 1988; Yılmazer and Karamanderesi, 1994; MTA, 1996; Hacıoğlu et al., 2019). Hydrogeological and hydrogeochemical studies around the study area have generally focused on geothermal fluid chemistry (Tarcan et al., 2000a; Tarcan et al., 2000b; Tarcan et al., 2003; Tarcan, 2005; Tarcan et al., 2005; Özen et al., 2009, Özen et al., 2012). Moreover, thermal waters have been used in residential heating for a long time in the region. The sustainability of the geothermal systems has a remarkable value. By preventing excessive fluid production and drilling more wells than required, geothermal system can be sustainable. Land subsidence may occur in the regions where excessive pumping is performed (Guo et al 2015; Taniguchi et al 2009). Considering all these, Kurşunlu geothermal field (KGF) is an important and convenient area for simulating numerical modeling of fluid flow and heat transfer. Based on the available data, numerical modeling of heat transport and fluid flow has been carried out in this geothermal area. The main goal of this study is to carry out the missing numerical modeling studies to illuminate possible fluid dynamics in the KGF. In this way, areas with the highest possible temperature can be discovered with a minimum expense, and sustainability can be achieved. This will shed light on the similar geothermal systems in the Aegean Region.

1.1. Geological and hydrogeological settings

KGF is located within the Menderes Massif, which occupies an important place among the graben systems of Western Anatolia. The Menderes Massif is divided into three sub-massifs: the northern, central, and southern boundaries of the Gediz and Büyük Menderes Grabens (Bozkurt and Oberhansli, 2001). The southern part of the Gediz Graben is an active half graben, and the graben was first formed by the movement of the Karadut fault, and, as a result of faulting in the deposition area, sediments of the Acıdere, Göbekli, Kurşunlu and Asartepe formations were deposited (Figure 1).

The Mesozoic (Lower Triassic-Upper Cretaceous) aged rocks of the Menderes Massif are composed of fine-grained gneisses, various schists (mica schists, garnet-

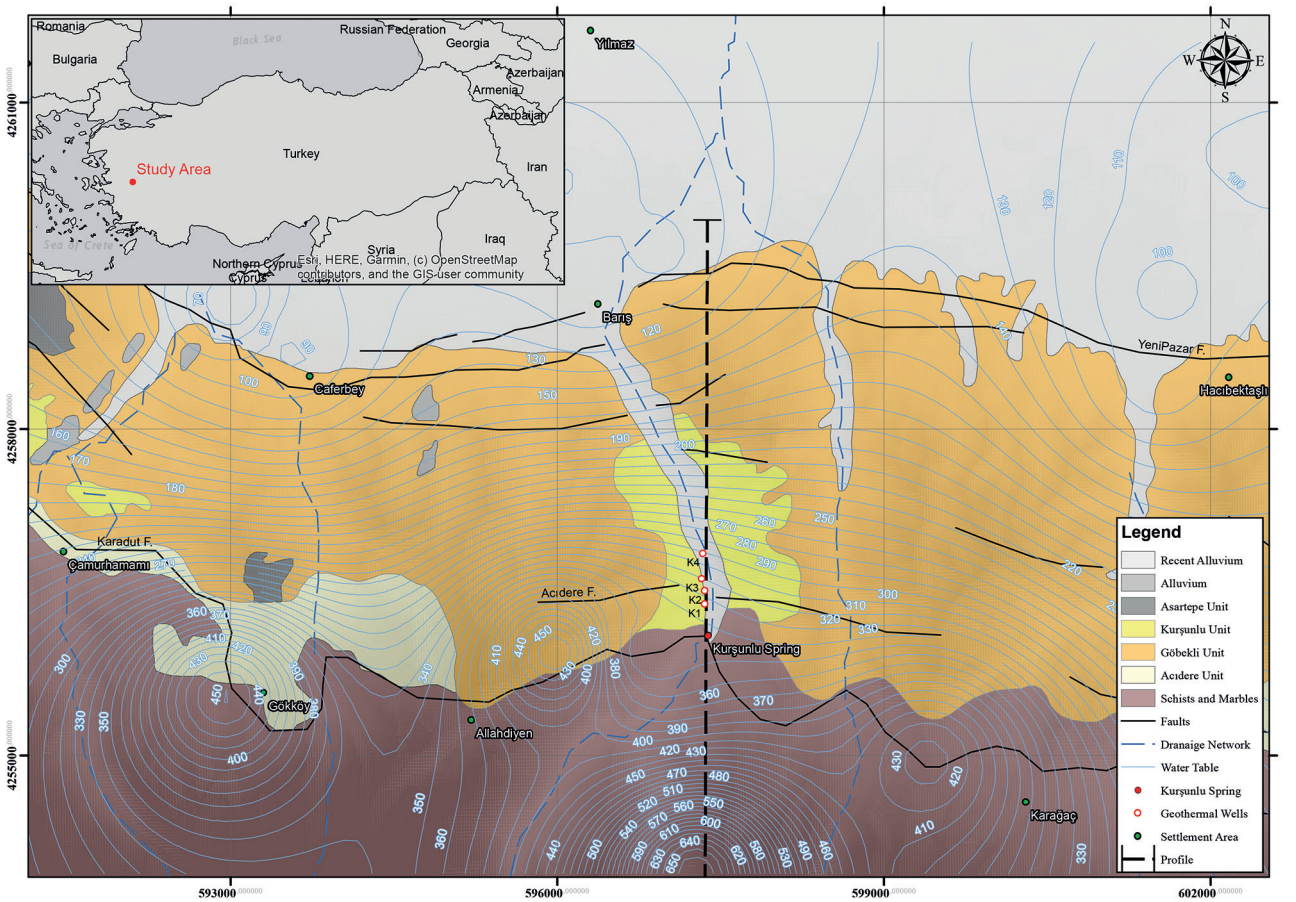

Figure 1. Geology and hydrogeology map of the study area and the cross-section line used in numerical modeling (Geology data is modified from Emre, 1990; hydrogeology data is from Özen, 2009).

mica schists, muscovite-quartz schists) and phyllites and metamorphic rocks such as meta quartzite and karstic marble and granodiorite formed by detachment or separation fault (Erdoğan and Güngör, 1992). The basement rocks composed of metamorphic and crystalline rocks of the Menderes Massif form the impermeable layer of the geothermal system.

Menderes Massif has been deformed many times starting from Paleocene for the first time (Gökten et al., 2001). As a result of these deformations, the fractured structures in the upper parts of the massif together with the carbonate levels formed the reservoir rocks of the geothermal system. At the same time, geothermal aquifers act as high permeable environments formed by numerous fault zones due to grabenization within the massif. Carbonated rocks within the Menderes Massif basement rocks act as an aquifer for thermal waters. Fractured parts of the gneiss and quartz–schist units are the aquifers of thermal waters as well. Mica–schists and phyllites are aquicludes because of their low permeability (Özen et al., 2012). Where low permeablity and impermeable rocks such as schist and phyllite units underlie the carbonated and fractured aquifers at depth, natural thermal springs discharge along faults and fractures (Tarcan et al., 2000).

Neogene Göbekli, Kurşunlu and Acıdere units, which are made up of granular alluvial fan deposits including poorly cemented clayey levels, have very low permeability and form the cap rocks of the geothermal systems. The shallow regional aquifer consists of Holocene alluvial deposits in the center of the study area. (Tarcan et al., 2000). The Acıdere, Göbekli, Kurşunlu, and Asartepe formations consisting of clastic sediments in KGF form the cap rocks (Emre, 1996a; Emre, 1996b).

The source of heat is the magma and geothermal gradient approaching the earth along the young faults connected to graben tectonics (Emre, 1990). Faults that are particularly abundant play a major role in the formation and development of longitudinal and transverse valleys (Roche et al., 2019). The Kurşunlu and Çamurhamamı geothermal fields are formed at the intersection of the north-sloping, left-strike normal faults and the low-angle Gediz fault. The offsets in these faults facilitate fluid flow and geothermal activity (Faulds et al, 2009). There are many hot water springs away from the main fractures that indicate the spread of geothermal fluid at regional scale.

2. Material and methods

FEFLOW commercial software was used in numerical modeling studies. FEFLOW is a simulation software for fluid flow and heat transfer that is fully associated by density dependent and finite element. It is designed to solve 2- or 3-dimensional flow, mass and heat transport. FEFLOW can solve thermohaline advection-dispersion equilibrium equations as well. This software is used in many areas such as mine water management, tunneling, agriculture, and geothermal energy.

2.1. Temperature logs

Among the drilled wells in KGF, four of them were selected and used in this study. Between the years 1976 and 1996, when the wells were drilled, the maximum well temperatures for K1, K2, K3, and K4 were 91, 94, 94 and 60 °C, respectively. The depths of the wells are 45, 70, 114, and 260 m, respectively. Measured temperature-depth profile and mud outlet temperature in the K4 well is shown in Figure 2 together with the lithology of the well. Decreasing in mud outlet temperatures is observed due to gas outlets around 100, 140 and 160 meters mostly in Miocene aged marble unit. Currently, K3 well is not used at all and K4 well is used for reinjection. The temperature of the wells varies widely depending on the season and usage conditions. During the summer, wells are not used for production and the system gets time to recover during the recovery period. Recently, K2 well is still used as a production well with a temperature of 74 °C, and the temperature of 6 out of 25 wells drilled in the region varies between 54–90 °C (Demirtaş et al., 2013). The Aegean region has an average heat flow of 110 mW/m^2 (İlkışık, 1995; Sarı and Şalk, 2003). Despite this large-scale data, the thermal gradient in the K4 well is quite high with a value of 20°C/100 m.

2.2. Profile

In order to reveal fluid flow dynamics and heat transport processes in KGF, a 2D vertical cross-section has been prepared (Figure 3). The selected profile located along the North-South direction to cover all the data gathered. The profile cuts four geothermal wells to be used for calibration purposes as well as the main fault zones. Impermeable rocks, cap rocks, and aquifers together with the fault zones are shown in the Figure 3. While KGF is located in the middle of the profile, Salihli district is located in the north part of profile. The southern end of the profile rises towards the Bozdağ horst region where the KGF is recharged. The aim is to have detailed information about possible transport processes in and around the geothermal aquifer.

Özen (2009) states that, according to the results obtained from geophysical data, the aquifer thickness consisting of marbles in the Caferbey region in the north of KGF varies between 250 and 2000 m. This thickness is between 100 and 800 m in Çamurhamamı region in the west of KGF, and it decreases down to 200 m in KGF. Only the first 10 m of the 200 m thick aquifer consists of a marble aquifer. There is no data about fault damage zones in KGF. The width of a damage zone varies in mm or m scale depending on the fault type. In KGF a 30 m zone on both sides of the faults is defined as fault damage zone.

Vertical electrical sounding methods, magnetic and self / spontaneous potential (sp) measurements in KGF

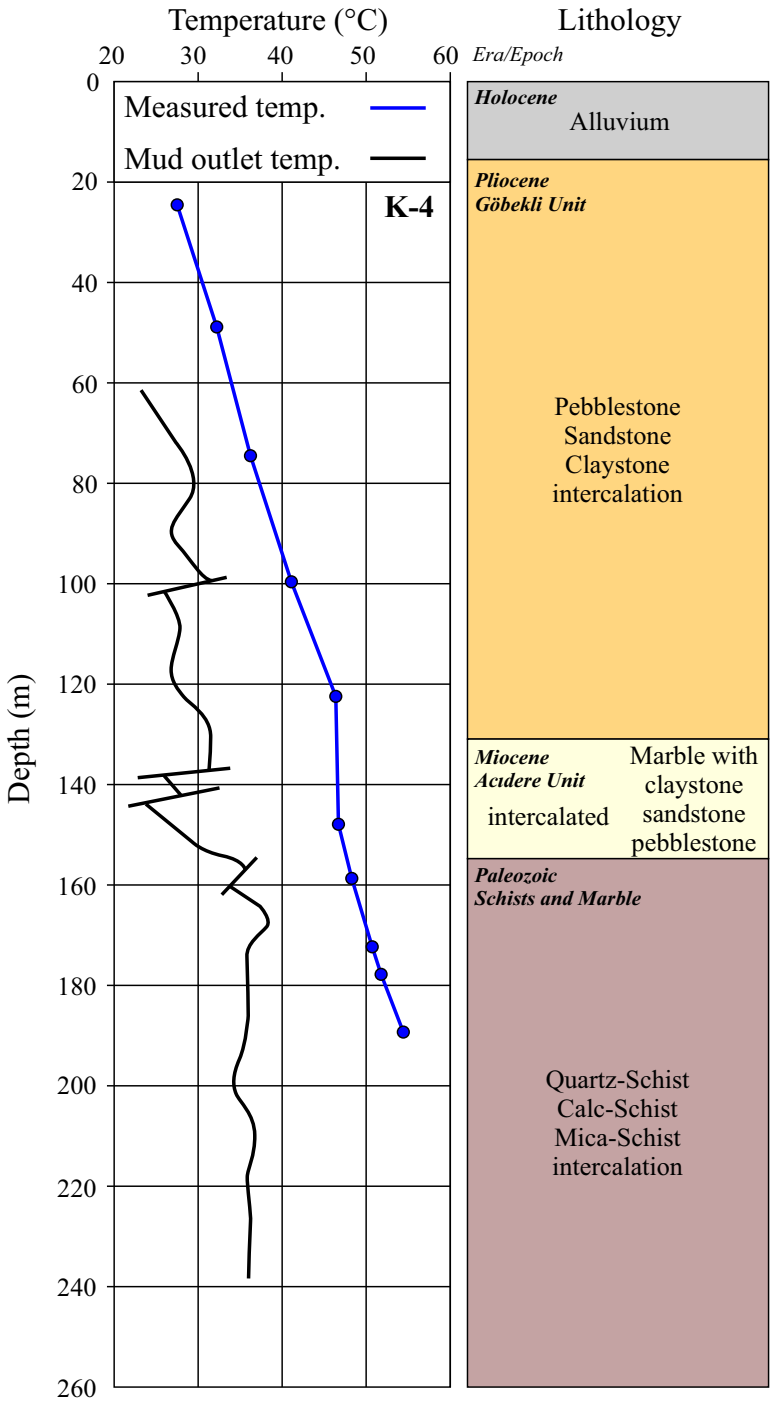

Figure 2. Measured temperature-depth profile, mud outlet temperature, and lithology in the K4 well (MTA Genel Müdürlüğü, 1996).

had been done by Temimhan (2006). It is mentioned that there is a low resistivity unit at depth of 200 m. It is determined that there are marble zones at these levels in the logs obtained from geothermal wells drilled in KGF.

According to Faulds et al. (2009), the reservoir rock is inclined to north along the normal faults; its depth varies between 10 and 200 m. In another study, it is mentioned that geothermal aquifer temperatures decrease towards the south (Yılmazer and Karamanderesi, 1994).

Considering the heat flow (Q), thermal conductivity (K) and geothermal gradient (G) data (Erkan, 2015; Göktürkler, 2003) of Western Anatolia, the profile was

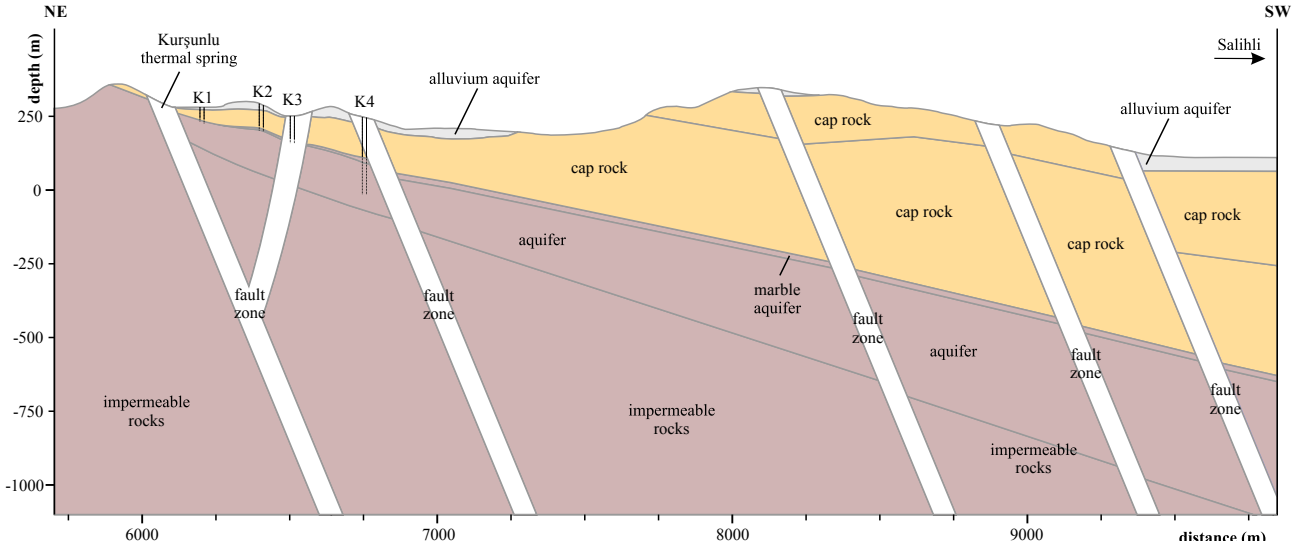

Figure 3. Hydrogeological parameters of Kurşunlu geothermal system (Modified from Oğuz, 2009).

selected as approximately 7 km on average at varying depths. The southern end of the whole selected profile starts in Bozdağ horst and continues to the alluvium in the north. It is approximately 10 km long. The model will be focused on geothermal aquifer in order to see the details easily throughout the whole manuscript.

2.3. Mesh structure

A Two-dimensional vertical model was built using the Delaunay method (Shewchuk, 1996) with a variable width of triangular mesh consisting of a total of 55590 elements and 28243 nodes (Figure 4). No holes are allowed within the triangular mesh. Since fluid flow and heat transfer calculations are made in each node, a denser mesh structure is required to be compared to other regions in order to follow the small-scale changes in possible areas where heat transfer may develop. Therefore, denser mesh was used along the fault zones. While the mesh resolution is a few meters at the edge of the units and fault zones, the mesh resolution reaches several hundred meters in the middle parts of the units.

As the physical borders of the geothermal aquifer are limited by impermeable rocks and since the fluids need a permeable zone to flow, all the fault zones in the area are designed to be permeable to achieve the recharging process.

2.4. Physical properties of units and fluids

Each unit in the model was evaluated as homogeneous in terms of its physical properties such as hydraulic conductivity, porosity, heat capacity, or thermal conductivity. These values have been obtained from previous geological, hydrogeological (tracer experiments, pumping tests), and geophysical studies such as Özen (2009), Erkan (2015), İlkışık (1995), Sarı and Şalk (2003), and Göktürkler et al. (2003).

Özen (2009) carried out pumping tests in wells drilled in the Kurşunlu cold water aquifer. In the study, values such as well coordinates, well depth and elevation, static and dynamic levels, flow rates, and temperatures are shared. It is also stated the aquifer parameters obtained as a result of the field studies. Accordingly, the hydraulic conductivity (K) of the aquifer was obtained as 6.9847×10^{-5} m/s, the transmissivity (T) as 2.794×10^{-3} m^2/s and the storativity (S) as $1.64x10^{-4}$.

The region has an average heat flow value of 110 mW/m^2 (İlkışık 1995; Sarı and Şalk 2003). Except for the hydraulic conductivity value, all these data obtained from previous studies were used in the model. The hydraulic conductivity values were used after being evaluated as the first predictive value in the PEST module. The details about PEST module will be given in calibration chapter. The parameters are presented in Table 1.

In all hydraulic calculations, the vertical velocity of groundwater is generally ignored because it is very low. The horizontal progression of groundwater is due to the larger horizontally dominant flow vectors. However, since it is estimated that the recharge of the Kurşunlu aquifer takes place at altitudes of 1500 m and reaches the aquifer as a result of a deep circulation, the anisotropy ratio was determined as $k_x:k_z$ = 1:1 in all units and faults except the aquifer. Dominant flow in the horizontal direction is allowed to mimic the aquifer unit consisting of intercalated lithology. Thus, it has been applied as $k_x:k_z$ = 10:1 for the aquifer. Considering the fluid properties of the KGF, it can be considered as a single-phase fluid flow (Özen, 2012).

2.5. Boundary and initial conditions

All lateral boundaries are set as no-flow boundaries in this model. Hydraulic heads and temperature values are defined on the top of the profile (Figure 5). The piezometric

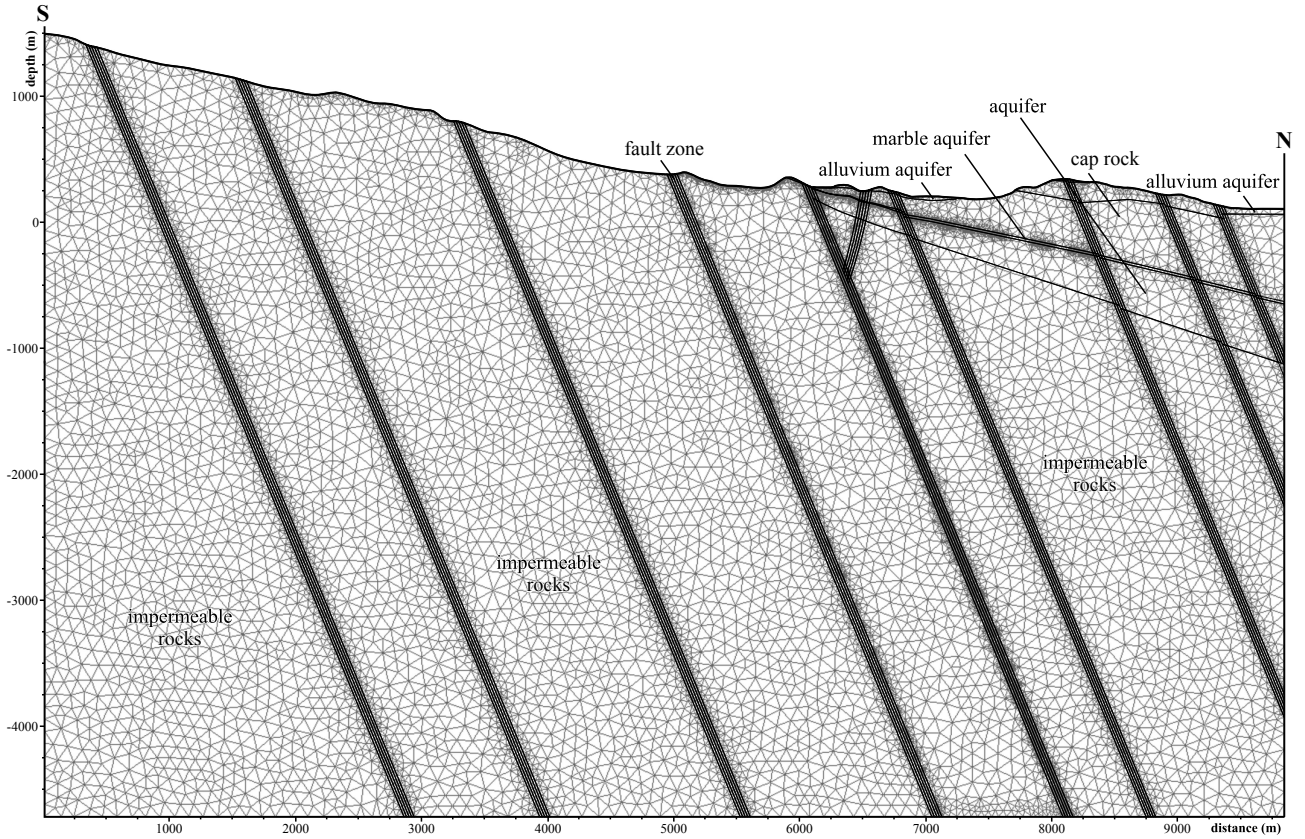

Figure 4. Finite element mesh created by triangulation (Delaunay) method (Shewchuk, 1996) for numerical modeling in the KGF.

Table 1. Physical parameter values assigned to elements.

	Hydraulic Conductivity (m/s)		Porosity	Heat Capacity ($J/m^3/K$)	Thermal Conductivity (J/m/s/K)
	Horizontal (k_x)	Vertical (k_z)			
Aluvium	4.4×10^{-2}	4.4×10^{-2}	0.5	1.7×10^{6}	1.5
Cap rock	1×10^{-9}	1×10^{-9}	0.005	2.1×10^{6}	3.0
Aquifer	1×10^{-4}	1×10^{-5}	0.3	2.52×10^{6}	2.8
Basement Rocks	3.33×10^{-11}	3.33×10^{-11}	0.05	2.1×10^{6}	3.5
Faults	1×10^{-4}	1×10^{-4}	0.7	3.0×10^{6}	2.0

surface was defined in the model using the data obtained from shallow wells drilled in the alluvial aquifer and deep wells drilled in the massif. Since there is no well data at the south end of the profile, the piezometric surface was estimated here in accordance with the topographic elevations. According to the data obtained from the deep wells drilled in the middle of the profile, the piezometric level varies between 320 and 655 m. On the north side of the profile, the groundwater table is approximately 100 m below the surface.

The Cauchy boundary condition has been applied in order for heat convection to take place on the surface of the profile. In this way, since the surface temperature will not be constant during the heat transfer process, it may increase or decrease. In the whole model, the reference temperature was defined as 16.5 °C degrees, which is the annual mean temperature (Tarcan et.al., 2000). According to Göktürkler et al. (2003), the average temperature value calculated for approximately 7 km depth is 250 C ± 20 °C. A constant 270 °C has been applied to the base of the model as a temperature boundary condition.

2.6. Model calibration, accuracy, and sensitivity analysis

This model is built on the initial conditions of the aquifer with data recorded after the completion of the geothermal

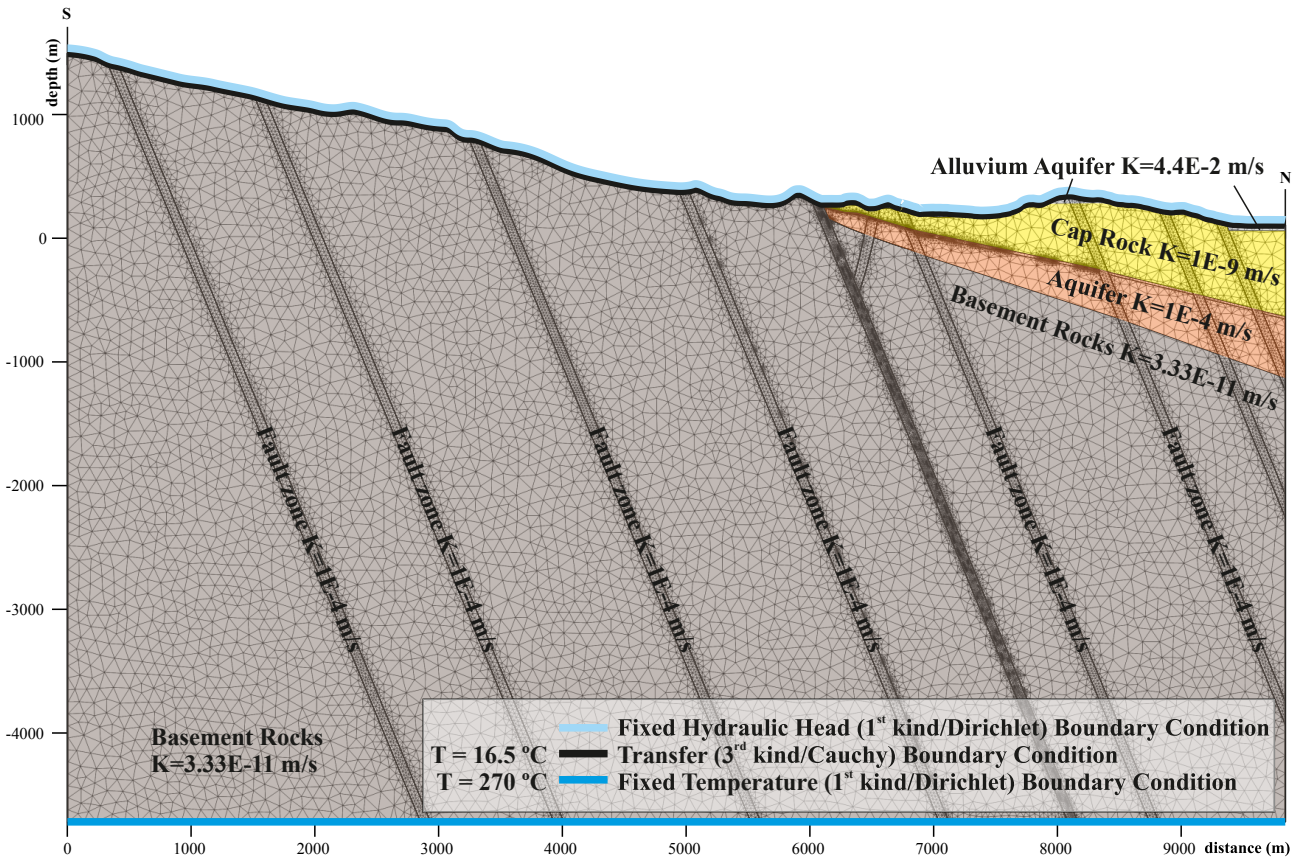

Figure 5. Conceptual model showing the boundary conditions and hydraulic conductivities.

wells. Temperatures, flow rates, and pressures vary according to the dry and rainy season and the state of use in the system, which is actively used in residential heating. The initial conditions have been chosen as temperature and pressure data was used in the calibration process.

The PEST (Parameter ESTimator) module embedded in the FEFLOW software was used for the calibration process. The required input data is provided with the PEST interface. The hydraulic conductivity parameter for groundwater flow was used for calibration process. Initial, lower, and upper boundary values are required for automatic estimation process. The PEST module runs the model many times for estimating or adjusting parameters. With the PEST module, automatic calibration is supported for steady-state groundwater flow models. After the parameter estimator process is accomplished, adjusted conductivity values for all units are presented in Table 1.

Regression analysis is used to check the accuracy of the model. The difference between calculated and observed value is defined as error. Root mean square error (RMSE) is the standard deviation of errors. The lowest RMSE value means the least errors. RMSE is calculated as follows:

$$RMSE = \sqrt{\sum_{i=1}^{n} \frac{(c_i - o_i)^2}{n}}$$

where

o: observed values

c: calculated values

n: sample size

Sensitivity analyzes were performed manually on hydraulic conductivity values under steady state conditions prior to the model run. Different hydraulic conductivity values were obtained by multiplying the hydraulic conductivity values by 0.2, 0.6, 1.0, 1.4, 1.8, 2.2, 2.6, and 3.0 to find the lowest RMSE value. The model was run once by multiplying the hydraulic conductivity values with a multiplication factor, and then a RMSE value was calculated for four observation points (o1-1, o1-2, o1-3 and o1-4).

The model has been run for about 700.000 days. Results are presented in Figure 6. The calculated well bottom temperatures stayed stable at the end of 300.000 days. Bottom well temperatures were calculated between

73 and 80 °C. When the wells were first drilled in 1976, the measured well bottom temperatures were between 60 and 90 °C. Since there is no temperature-depth data except for the K4 well, the maximum well bottom temperatures were used in the calibration process. Calculated temperature-depth results are given in Figure 6. In order to check model accuracy RMSE value is calculated using calculated and observed values given in Table 2.

Scatter plot of calculated and observed values for hydraulic head is given in Figure 7.

The lowest RMSE value calculated as 3.2 was obtained by multiplying the hydraulic conductivity values by a multiplying factor of 1.8 (Table 3).

Figure 8 shows the sensitivity analysis results. The value of the calculated errors started to decrease after the multiplier of 1.4 and the lowest error was obtained at the multiplier of 1.8. It was observed that the calculated errors for low and high multiplier values are very high.

3. Results

Initial condition values for hydraulic head and heat transfer calculations were produced under steady-state conditions. The data produced under steady-state conditions were used to create a transient model. The flow and heat transfer model was run for approximately 700,000 days.

3.1. Flow model

Firstly, the flow model was run in the absence of geothermal gradient. With topography driven flow, main groundwater flow direction is from Bozdağ towards Salihli direction (Figure 4). The groundwater flow coming from Bozdağ direction moves down just after it is met with the southern flank of the fault. Groundwater flow captured by the fault is transferred deeper (Figure 9). Approaching the fault zones, the flow paths lose their straight-line form due to the sudden pressure changes. The pressure values continue to decrease as they approach the fault zones towards the north. The groundwater, which maintain this flow pattern until the area where the Kurşunlu geothermal spring is located, after reaching the fault zone, move towards the surface and forms the Kurşunlu geothermal spring. Unlike the flow pattern in the faults in the south of the Kurşunlu spring, the faults in the north of the spring raise the fluids towards the aquifer within the faults and after reaching the geothermal aquifer, it heads towards the Kurşunlu geothermal spring and reaches the surface. It is seen here that the faults are hydraulically connected with

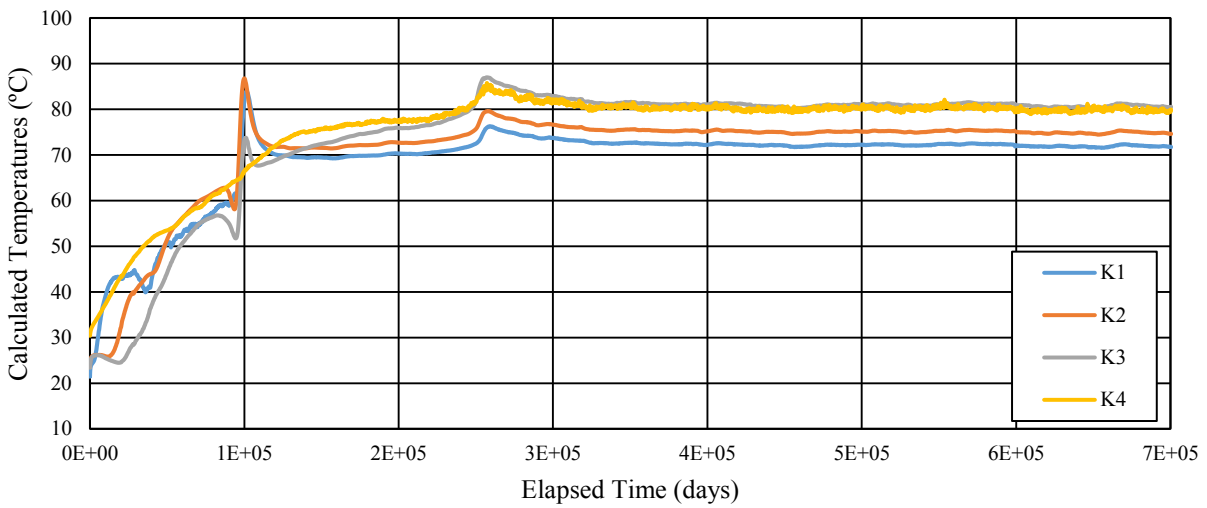

Figure 6. Calculated well bottom temperature values in wells K1, K2, K3, and K4.

Table 2. Observed, calculated values, and RMSE values of observation points.

Observation Point	Observed Value (m)	Calculated Value (m)	Error	Squared Error	Sum of Squared Error	Mean of Squared Error	RMSE
o1-1	640	635.191	4.81	23.13	40.93	10.23	3.20
o1-2	280	278.740	1.26	1.59			
o1-3	100	100.463	–0.46	0.21			
o1-4	96	100.000	–4.00	16.00			

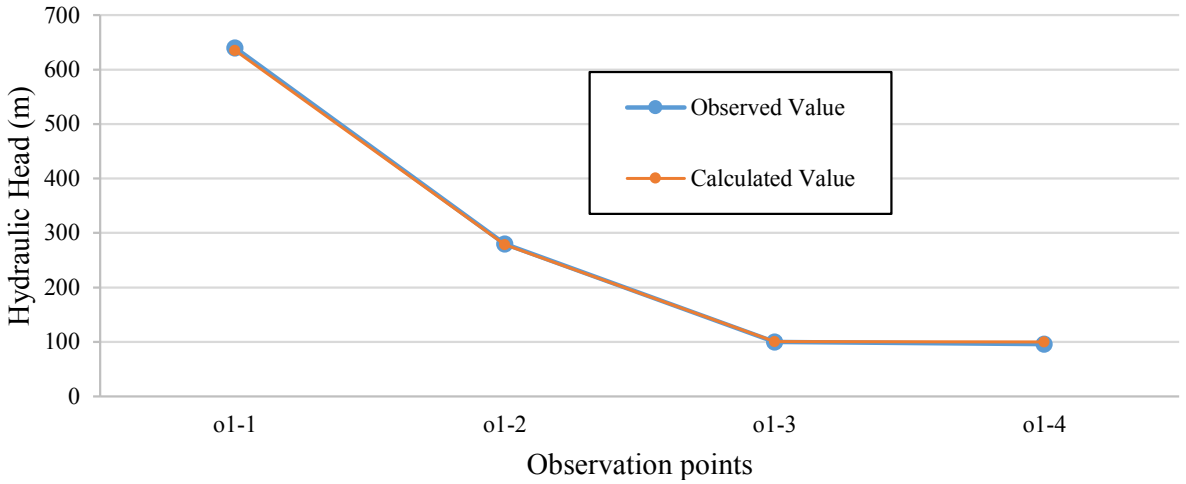

Figure 7. Scatter plot of measured and calculated values.

Table 3. Calculated RMSE results according to multiplier factors.

Observation Point	×0.2	×0.6	×1.0	× 1.4	×1.8	×2.2	×2.6	×3.0
o1-1	4.809	4.808	4.809	4.809	4.809	4.809	4.809	4.809
o1-2	–12.382	–12.331	–12.335	8.959	1.26	–12.312	–11.641	-12.314
o1-3	–1.61	–1.915	–1.979	–0.029	–0.463	–2.084	–7.02	–2.059
o1-4	–4.00	–4.00	–4.00	–4.00	–4.00	–4.00	–4.00	–4.00
RMSE	6.98	6.98	6.99	5.46	3.20	6.98	7.48	6.98

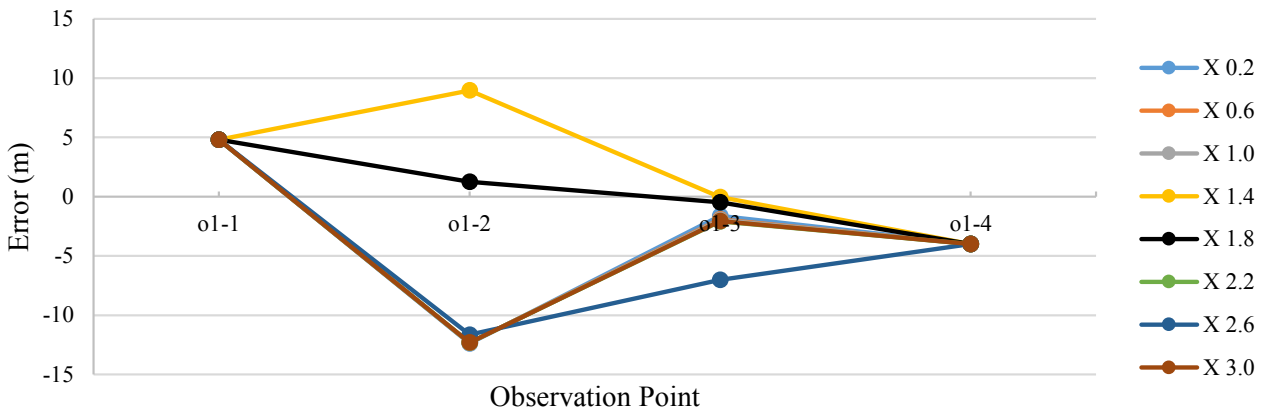

Figure 8. Sensitivity analysis results.

each other. Groundwater flows from Bozdağ region where hydraulic heads are the highest to the north direction. The groundwater divide has not been observed in this section of study area; however, it is expected to be at the southern boundary of the model.

3.2. Flow and heat transfer model

Following the completion of the flow model, a heat transfer model was started to build. Figure 10 shows the calculated flow paths with the effect of geothermal gradient. It was observed that convective flows started to occur in the bedrock at –4000 m altitude at the south end of the profile. The groundwater flow infiltrates the fault zone from the southern flank of the faults, similar to the flow model on the southern side of the profile. Approaching the Kurşunlu spring, the convective flows in the bedrock, especially between –3000 and –4000 m altitudes are remarkable.

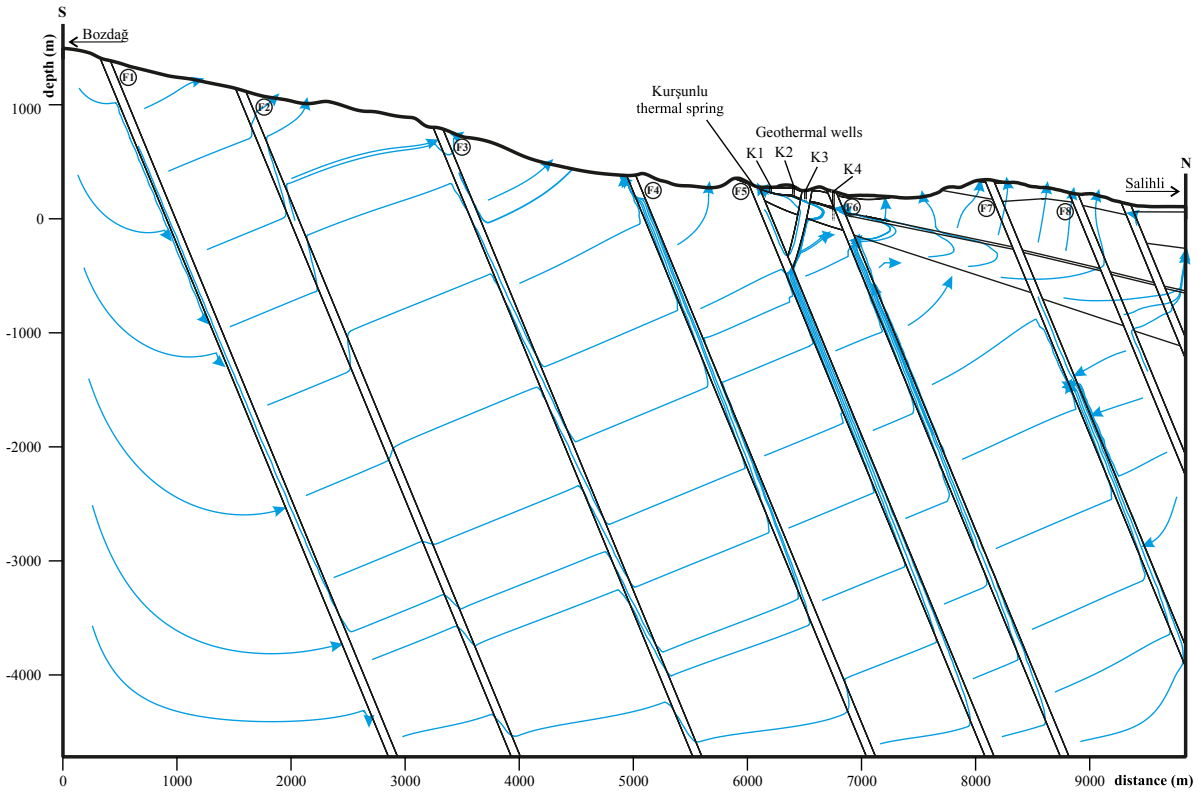

Figure 9. Calculated flow path in the absence of geothermal gradient in Kurşunlu geothermal system.

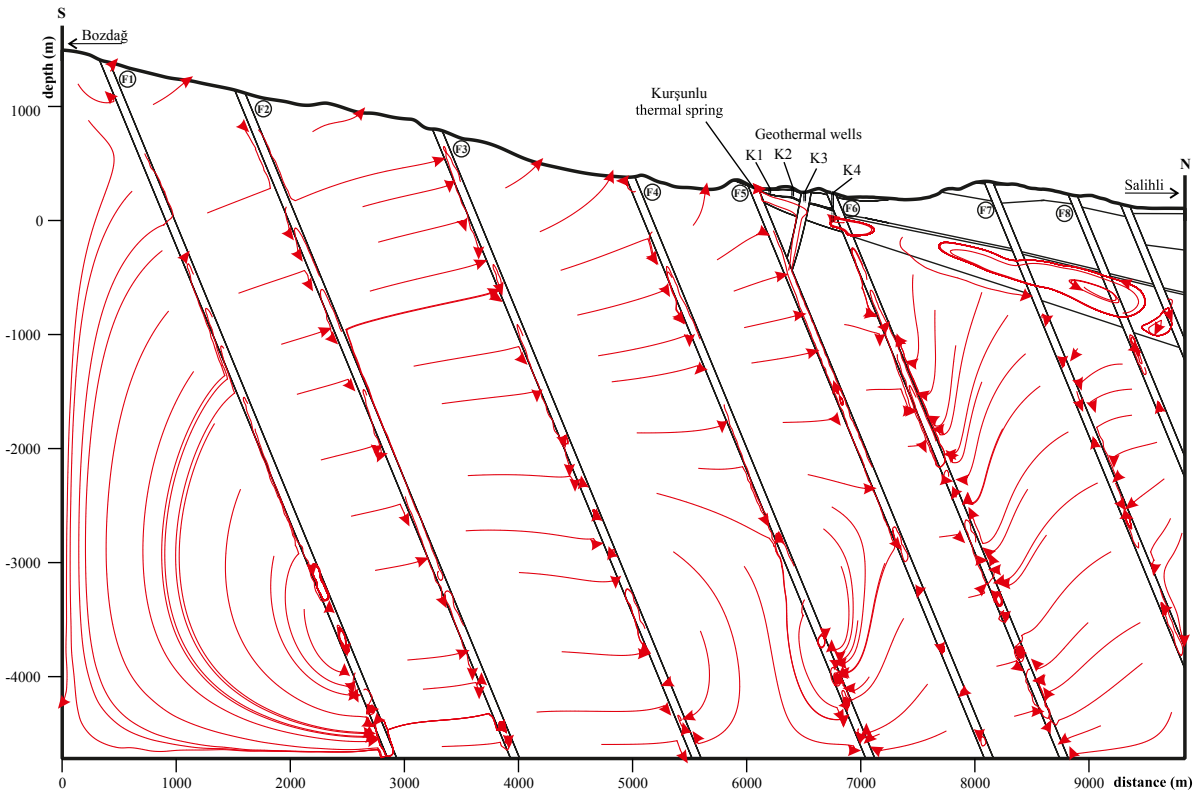

Figure 10. Calculated flow paths with the effect of geothermal gradient in Kurşunlu geothermal system.

In the geothermal aquifer, widespread convective flows in deeper regions were formed, while smaller spread convective flows were formed near the surface and shallow depths (Figure 10). Heated fluids reach the surface before convective flows start to form in the closest and shallowest region to the Kurşunlu spring. On the other hand, in the fault zones (F1, F2, F3, F4, F5 and F6), convective flows form at different depths independently of each other (Figure 11). Convective flows begin to form in fault zones F1 and F2 and fault zone F6 at altitudes of –3000 m on the south side and –1500 m on the north side of the profile, respectively. Unlike the flow model, the south dipping fault located just north of the Kurşunlu spring captures heated fluids from both the southern and northern flanks of the fault zone and transfers them to the surface.

Cold-water inflow occurs in fault zones (F1, F2, F3 and F4) in the south direction of the profile, including the fault (F5) itself on which the Kurşunlu thermal spring is located (Figure 11). Only in two of these faults (F2 and F3), possible thermal spring outflows are seen at distances of 300–500 m away from the northern flank of the faults. In another third fault zone (F4), neighboring the fault zone in which Kurşunlu thermal spring is located, the heated fluids rise almost to the surface. In these three fault zones (F2, F3, and F4), thermal water can still be obtained directly from the fault zone at a low expense, even if the fluids do not actually reach the surface. It is seen that the thermal waters that can be obtained from these fault zones at depths of 500 m on fault F2 and 600 meters on fault F3 may have a higher possibility of around 150 °C compared to those obtained from the KGF (Figure 12).

Figure 13 presents the pressure distributions obtained from the flow and heat transfer model. The pressure lines mimic the topography in the shallow parts of the profile where the pressure values are relatively closer to the surface pressure. Pressure values begin to change in all fault zones after 2000 m of depth and lose their topography-like forms. This change is more evident in the south of the section. Starting from the altitudes of –1500 m, as the depth increases, the change in the sudden pressure drops seen in the fault zones (F1, F2, F4, and F6) increases significantly. The pressure drop in the fault zone (F3) is enormous. Conversely, an increase in pressure is observed in the fault zones (F5, F7, and F8) at the altitudes of –2500 m.

On the other hand, sudden pressure drops are observed in the fault zones. While the pressure lines present a

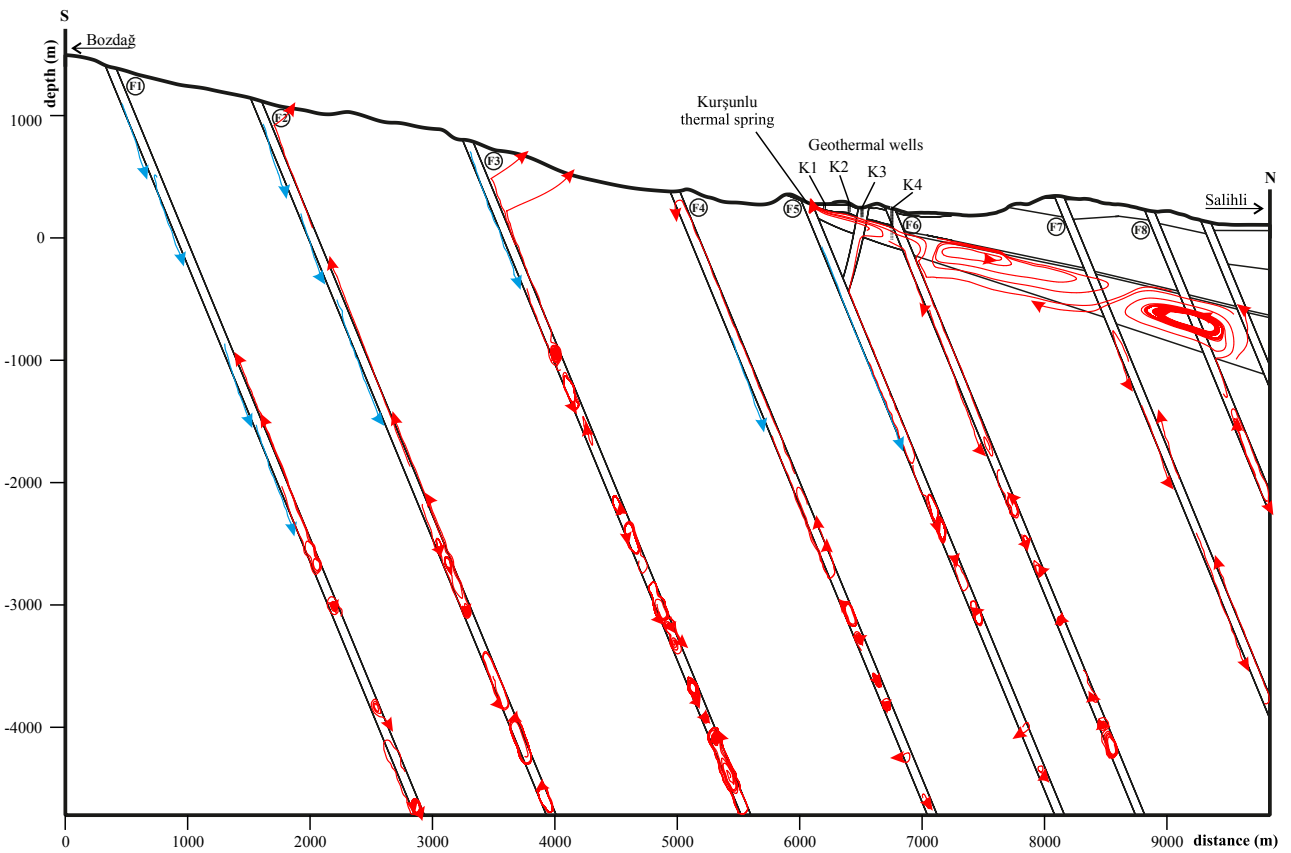

Figure 11. Calculated flow paths in the fault zones. Blue lines stand for infiltrating cold water and red lines stands for heated fluids and convective flows in the aquifer, respectively.

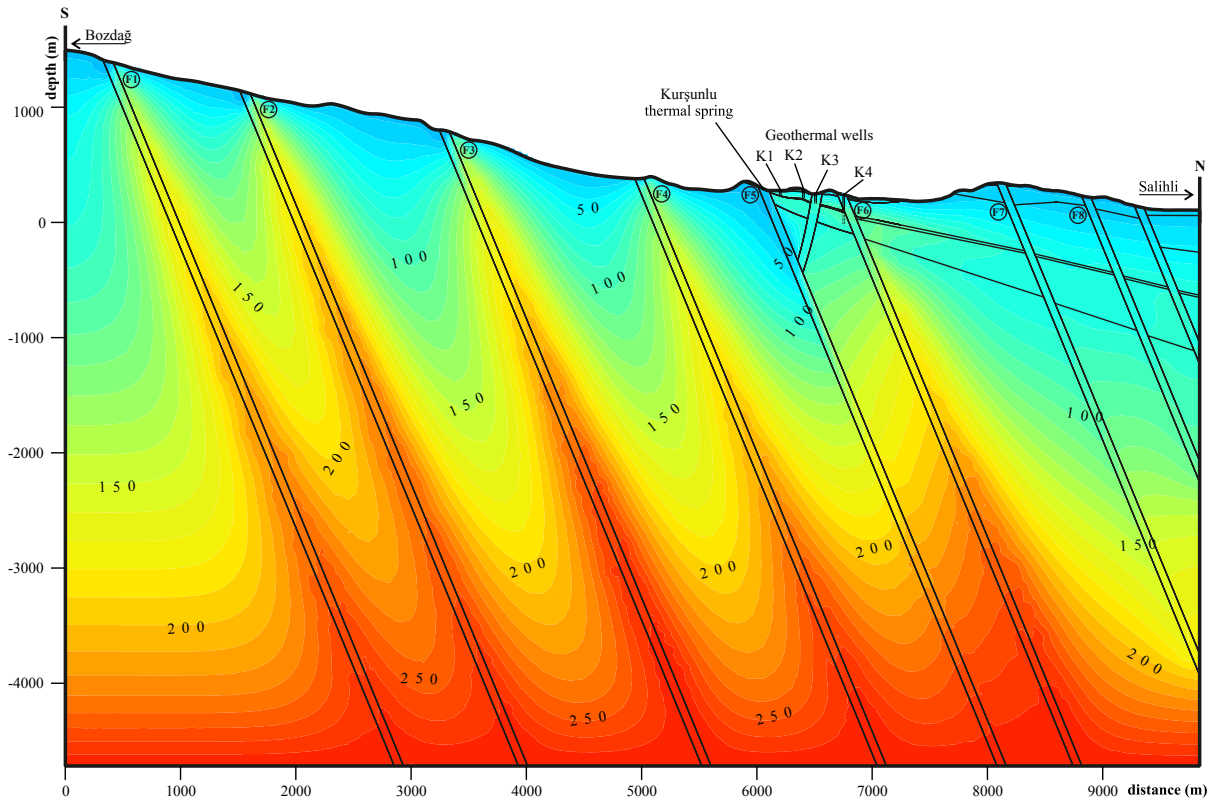

Figure 12. Calculated temperature (°C) distribution.

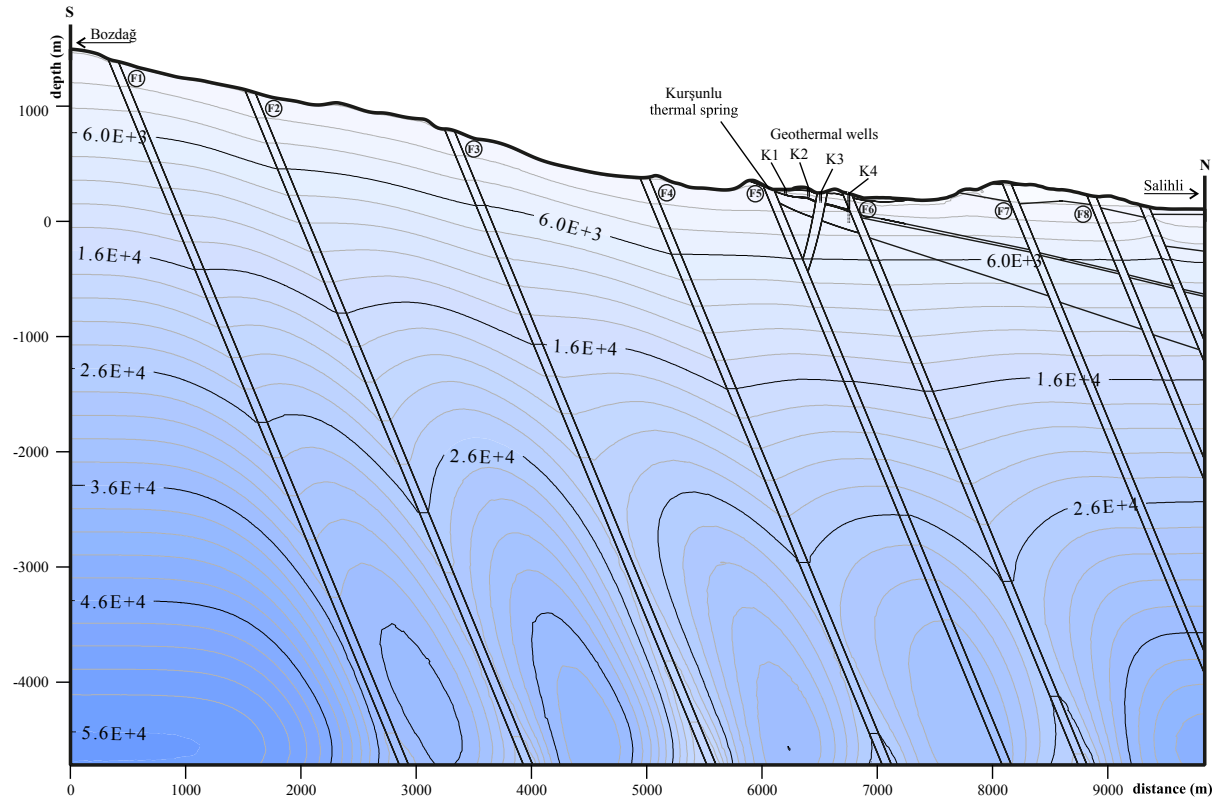

Figure 13. Calculated pressure (MPa) distribution.

straight line in the upper parts of the profile, the flow paths are in a straight form in the fault zones. When evaluating the heat transfer, flow path, and pressure distribution figures together while the pressure lines present a straight line in the upper parts of the profile, the flow paths are in a straight form in the fault zones (Figure 14).

However, it is also observed that convective flows occur in the fault zones where sudden pressure drops take place. When these sudden pressure drops in the fault zones are mapped, suitable areas for reinjection, which is mandatory for geothermal regions, can be explored more easily. Low pressure zones can be used for reinjection process at a low cost.

Temperature changes were calculated on the red dashed line in the cross-section shown in Figure 15. The goal in choosing this line is to observe temperature changes along a direction that cuts the geothermal aquifer. This line is located approximately 80 m above the mean sea level. According to the Figure 15 groundwater flows towards the fault zone with a temperature of 20 °C from the southern flank of the fault zone on which the Kurşunlu thermal spring is located, its temperature reaches up to 90 °C when it reaches the north flank of another neighboring north dipping fault. Fluids reaching the fault zone move towards the depths of the fault due to both convective currents and pressure in the fault zone. During this time, the heated fluid mixes with the relatively cold groundwater in the fault zone, losing about 70 °C of its temperature, and heads back towards the neighboring fault in the north. From south to north along the section, fluids approach the fault zone and heat up. When the fluid leaves the fault zone, it loses some of their heat. The fluids get closer to the next fault zone and heated up again. This cycle repeats itself in this way towards the north. The temperature of the fluid leaving the fault zone in which the K4 numbered well is located starts to decrease and stabilizes around 30 °C.

4. Conclusion

Since the recharging of the KGF is controlled by graben systems, it has the characteristic of a cyclic system, which can be explained as the precipitation water falling into recharging area by filtering through the cracks, heating in depth and surfacing by following the tectonic lines. For this reason, a strong interaction occurs between cold meteoric recharge and hot fluid rising by warming up in fault zones. As a result of this interaction, convection flows are formed. Temperature profiles show that the shallow reservoirs are affected by the increasing fluid temperatures due to the rising heated fluid.

A 2D flow and heat transfer model was built to reveal fluid flow dynamics and heat transport processes in KGF. The groundwater flow starts to infiltrate the fault zone from the southern flank of the faults, on the southern side of the profile. The regional flow direction is towards to the North. Fluid transport within the system takes place in hydraulically connected fault zones. It has been observed that the fluids are both transmitted deeply and heated through fault zones and transported towards the surface. Approaching the Kurşunlu spring, the convective flows form in the bedrock, especially between –3000 and –4000 m altitudes. Convective flows start to form below –1000 m altitudes in the fault zones as well. Flow paths in and around the Kurşunlu geothermal aquifer have been revealed. If two possible thermal wells with a 500–600 m depth, which cut the F2 and F3 faults, can be drilled, it may be possible to reach a temperature of 150 °C degrees. The temperatures of these wells seem to be higher than the temperatures reached in KGF. Furthermore, sudden

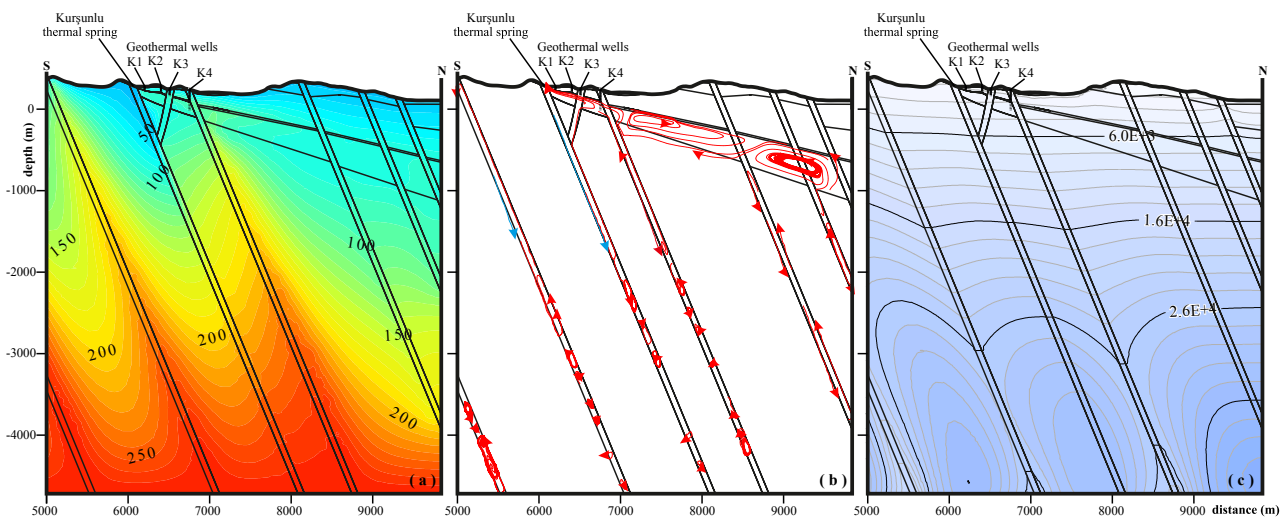

Figure 14. Close-up view of heat distribution (a), flow paths (b), and pressure distribution (c).

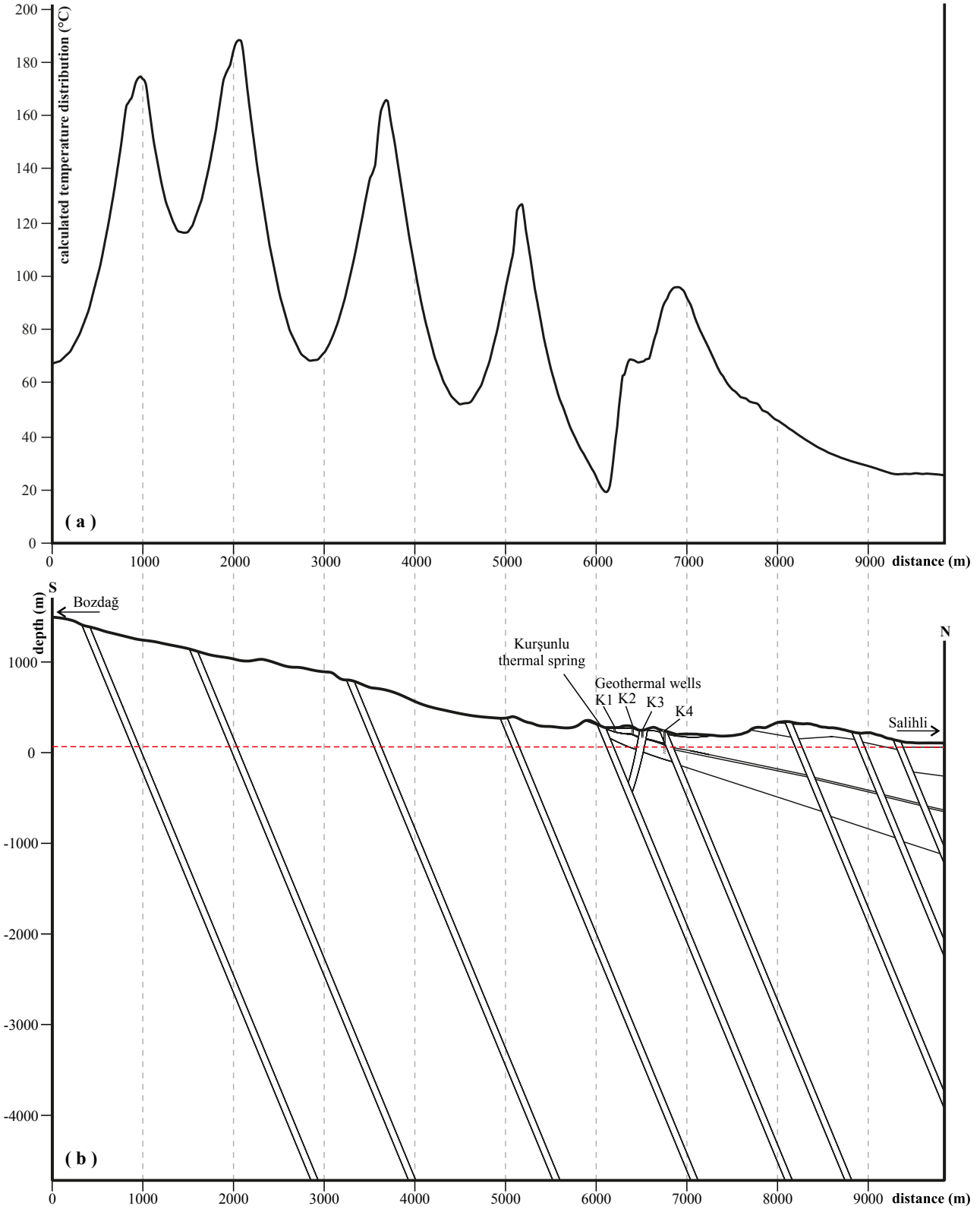

Figure 15. Calculated temperature (°C) distribution (a) around fault zones along the red colored section line (b).

pressure drops are observed where convective flows occur. These areas, where pressure drops occur, are very suitable for reinjection wells in geothermal regions. It will be possible to perform reinjection process in low pressure areas occurring in fault zones with a minimum cost.

Acknowledgments
This research was funded by the Department of Scientific Research Project Unit (BAP) of Dokuz Eylül University with the Project number of 2012.KB.FEN.076.

References

Bozkurt E, Oberhänsli R (2001). Menderes Massif (Western Turkey): structural, metamorphic and magmatic evolution-a synthesis. The International Journal of Earth Sciences 89: 679-708.

Demirtaş R, Özdemir A, Arabacı F, Şahin B (2019). Salihli-Bozdağ (Manisa-İzmir) Jeotermal Ruhsat Alanları Jeolojik Etüt Raporu. Ankara, Türkiye: (in Turkish). doi: 10.13140/RG.2.2.35914.00969

Dora OÖ, Candan O, Dürr S, Oberhanslı R (1997). New evidence on the geotectonic evolution of the Menderes Massif. In: International Earth Sciences Colloquium on the Aegean Region; İzmir, Güllük, Turkey pp. 53-72.

Economides MJ, Nolte KG (2000). Reservoir Stimulation, 3rd edition, England: John Wiles & Sons Ltd.

Emre T (1988). Gediz grabeni (Salihli-Alaşehir arası) karasal tortullarının yaşıyla ilgili yeni bulgular. In: 42. Türkiye Jeoloji Kurultayı Bildiri Özleri; Ankara, Turkey pp. 34-35 (in Turkish).

Emre T (1990). Sart Mustafa (Salihli) - Adala - Dereköy (Alaşehir) Arasının Jeolojisi ve Gediz Grabeninin Yapısına Bir Yaklaşım: TÜBİTAK Temel Bilimler Araştırma Grubu, Proje No: TBAG-732 / YDBAG-0001, (in Turkish).

Emre T (1996a). Gediz Grabeni'nin jeolojisi ve tektoniği. Turkish Journal of Earth Sciences (5): 171-185 (in Turkish).

Emre T (1996b). Gediz Grabeni'nin tektonik evrimi. Türkiye Jeoloji Bülteni 39 (2): 1-18 (in Turkish).

Emre T, Sözbilir H (1997). Field evidence for metamorphic core complex, detachment faulting and accomodation faults in the Gediz and Büyük Menderes Grabens, Western Anatolia. In: International Earth Sciences Colloquium on the Aegean Region; İzmir, Güllük, Turkey pp. 73-93.

Erdoğan B (1990). İzmir-Ankara zonu ile Karaburun tektonik kuşağının ilişkisi. Maden Tetkik ve Arama Dergisi 110: 1-15 (in Turkish).

Erdoğan B, Güngör T (1992). Menderes Masifi'nin kuzey kanadının stratigrafisi ve tektonik evrimi. Türkiye Petrol Jeologları Derneği Bülteni 4 (1): 9-34 (in Turkish).

Faulds JE, Bouchot V, Moeck I, Oğuz KK (2009). Structural controls on geothermal systems in western Turkey: A preliminary report. Geothermal Resources Council Transactions 33: 375-381.

Gökten E, Havzaoğlu Ş, Şan Ö (2001). Tertiary evolution of the central Menderes Massif based on structural investigations of metamorphics and sedimentary cover rocks between Salihli and Kiraz (western Turkey). International Journal of Earth Sciences 89: 745-756. doi: 10.1007/s005310000099

Göktürkler G, Şalk M, Sarı C (2003). Numerical modeling of the conductive heat transfer in western Anatolia. Journal of the Balkan Geophysical Society 6 (1): 1-15.

Guo H, Zhang Z, Cheng G, Li W, Li T et al. (2015). Groundwater derived land subsidence in North China Plain. Environmental Earth Sciences 74: 1414-1427.

Hacıoğlu Ö, Başokur AT, Diner Ç, Nedbel N, Arslan Hİ et al. (2020). The effect of active extensional tectonics on the structural controls and heat transport mechanism in the Menderes Massif geothermal province: Inferred from three-dimensional electrical resistivity structure of the Kurşunlu geothermal field (Gediz Graben, western Anatolia). Geothermics 85: 101708. doi: 10.1016/j.geothermics.2019.07.006

Hetzel R, Passchier CW, Ring U, Dora OÖ (1995a). Bivergent extension in orogenic belts: The Menderes Massif (southwestern Turkey). Geology 23 (5): 458-544.

Hetzel R, Ring U, Akal C, Troesch M (1995b). Miocene NNE-Directed extentional unroofing in the Menderes Massif, Southwestern Turkey. Geological society of London Journal 152: 639-654.

Hochstein MP (1990). Classification and assessment of geothermal resources. In: Dickson MH and Fanelli M (editors) Small geothermal resources, UNITAEWNDP Centre for Small Energy Resources; Rome, Italy pp. 31-59.

İlkışık OM (1995). Regional heat flow in western Anatolia using silica temperature estimates from thermal springs. Tectonophysics 244: 175-184.

Hofmann H, Blöcher G, Börsing N, Maronde N, Pastrik N et al (2014). Potential for enchanced geothermal systems in low permeability limestones - stimulation strategies for the Western Malm karst (Bavaria). Geothermics 51: 351-367.

Magri F, Akar T, Gemici Ü, Pekdeğer A (2011). Numerical investigations of fault-induced seawater circulation in the Seferihisar-Balçova geothermal system, western Turkey. Hydrogeology Journal 20: 103-118. doi: 10.1007/s10040-011-0797-z

MTA Genel Müdürlüğü (1996). Türkiye jeotermal envanteri: Ankara, Türkiye: MTA Genel Müdürlüğü Yayını, (in Turkish).

Oğuz KK (2009). Kurşunlu (Salihli) jeotermal alanındaki üretim ve geri basım kuyularının mineral dengeleri ve kabuklaşma eğilimleri. Msc, Dokuz Eylül University, İzmir, Turkey, (in Turkish).

Özen T (2009). Salihli Jeotermal Alanlarının Hidrojeolojik ve Hidrojeokimyasal İncelenmesi. PhD, Dokuz Eylül University, İzmir, Turkey, (in Turkish).

Özen T, Bülbül A, Tarcan G (2012). Reservoir and hydrogeochemical characterizations of geothermal fields in Salihli, Turkey. Journal of Asian Earth Sciences 60: 1-17.

Roche V, Bouchot V, Beccaletto L, Jolivet L, Guillou-Frottier L et al (2019). Structural, lithological, and geodynamic controls on geothermal activity in the Menderes geothermal Province (Western Anatolia, Turkey). International Journal of Earth Sciences (Geol Rundsch) 108: 301-328. doi: 10.1007/s00531-018-1655-1

Saemundsson K, Axelson G, Steingrimsson B (2009). Geothermal Systems in Global Perpective. In: Short Course on Surface Exploration for Geothermal Resources; Ahuachapan and Santa Tecla, El Salvador pp. 1-14.

Sarı C, Şalk M (2003). Heat Flow Investigations in Western Anatolia. In: Geophysical Research Abstracts, EGS-AGU-EUG Joint Assembly v5, 8509, Nice, France.

Serpen Ü (2004). Hydrogeological investigations on Balçova geothermal system in Turkey. Geothermics (33): 309-335.

Seyitoğlu G (1996). Ege'nin Geç Senozoyik K-G yönlü genleşmeli tektoniği: Bölgesel tektonik ve volkanik evrim modelleri üzerine bir tartışma. In: 49. Türkiye Jeoloji Kurultayı, Bildiri özleri, Ankara, Türkiye; pp. 31-33 (in Turkish).

Shewchuk JR (1996). Triangle: Engineering a 2D quality mesh generator and Delaunay triangulator. In: M.C. Lin and D. Manocha, Editors, Applied Computational Geometry: Towards Geometric Engineering, First ACM Workshop on Applied Computational Geometry Lecture Notes in Computer Science 1148; Berlin, Germany; pp. 203-222.

Simms MA, Garven G (2004). Thermal convection in faulted extensional sedimentary basins: theoretical results from finite element modeling. Geofluids 4: 109-130.

Taniguchi M, Shimada J, Fukuda Y, Yamano M, Onodera S et al (2009). Anthropogenic effects on the subsurface thermal and groundwater environments in Osaka, Japan and Bangkok, Thailand. Science of the total environment 401: 3153-3164.

Tarcan G (2005). Mineral saturation and scaling tendencies of waters discharged from wells (>150°C) in geothermal areas of Turkey. Journal of Volcanology and Geothermal Research 142: 263-283.

Tarcan G, Gemici Ü, Aksoy N. Hydrogeological and geochemical assessments of the Gediz Graben geothermal areas, western Anatolia, Turkey. Environmental Geology 2005; (47): 523-534.

Tarcan G, Filiz S, Gemici Ü (2000). Geology and Geochemistry of the Salihli Geothermal Fields, Turkey. In: WGC-2000 World Geothermal Congress, Books of Proceedings; Kyushu-Tohoku, Japan; pp. 1829-1834.

Tarcan G, Gemici Ü (2003). Water geochemistry of the Seferihisar geothermal area, İzmir, Turkey. Journal of Volcanology and Geothermal Research 126: 225-242.

Tarcan G, Gemici Ü (2005). Effects of the contaminants from Turgutlu-Urganlı thermomineral waters on the cold ground and surface waters. Bulletin of Environmental Contamination and Toxicology 74 (3): 485-492.

Temimhan S (2006). Salihli - kurşunlu kaplıcaları ve civarının jeotermal potansiyelinin araştırılması. Msc, Dokuz Eylül University, İzmir, Turkey.

Yılmazer S (1988). Kurşunlu-Sart sıcak su kaynaklarının (Salihli) hidrojeoloji ve jeokimyasal özellikleri. Isparta Mühendislik Fakültesi Dergisi 5: 242-266 (in Turkish).

Yılmazer S, Karamanderesi İH (1994). Kurşunlu jeotermal alanının (Salihli-Manisa) jeolojisi ve jeotermal potansiyeli. In: Dünya Enerji Konseyi, Türkiye 6. Enerji Kongresi, Türk Milli Komitesi; İzmir, Turkey; pp. 68-181 (in Turkish).